PHYSICAL REVIEW B **84**, 094512 (2011)

Pressure gradients in solid ^{4}He: Thermal quenching and annealing

A. Suhel and J. R. Beamish
Department of Physics, University of Alberta, Edmonton, Alberta, Canada, T6G 2E1
(Received 29 June 2011; published 14 September 2011)

Torsional oscillator measurements on solid ^{4}He show a frequency increase at low temperatures that suggests mass decoupling or nonclassical rotational inertia (NCRI). The magnitude of the NCRI appears to be larger when the helium is frozen and cooled rapidly. Annealing at high temperatures usually reduces the NCRI, with an accompanying drop in pressure, suggesting that defects are involved. Measurements in quenched or deformed crystals show a T^2 term in the temperature dependence of the pressure which has also been attributed to defects. We have built a cell with two capacitive gauges to measure the temperature dependence of the pressure and the magnitude of pressure gradients in solid helium. The helium can be melted in a few seconds using a heater embedded in the crystal and can be refrozen and quenched to low temperature very rapidly. From the maximum pressure differences in the cell, we infer a yield stress of order 4 kPa for solid ^{4}He near melting. The pressure gradients relax when the temperature is raised above about 0.5 K via a thermally activated annealing process with an activation barrier of about 5 K. The existence of significant pressure gradients makes it difficult to measure the thermodynamic temperature dependence of the pressure, for example to extract information about glassy regions or other defects.

DOI: 10.1103/PhysRevB.84.094512 PACS number(s): 67.80.bd, 67.80.dj

I. INTRODUCTION

The possibility of supersolidity—the coexistence of crystalline order and superflow—was suggested more than 40 years ago[1–3] but it was not until 2004 that Kim and Chan's torsional oscillator experiments[4,5] provided direct evidence of supersolid behavior in helium. At temperatures below about 200 mK, they observed an increase in the frequency of a torsional oscillator (TO) filled with solid ^{4}He, which they interpreted as a superfluidlike decoupling of about 1% of the solid—the nonclassical rotational inertia (NCRI) which characterizes a supersolid. Two other observations provided important support for this interpretation. First, the apparent decoupling decreased at high oscillation amplitudes, suggesting a critical velocity for superflow like that seen in superfluid helium. Second, blocking the annular channel eliminated the decoupling, confirming that long-range flow was involved. It soon became clear that this behavior must involve defects. Rittner and Reppy[6] showed that annealing (which removes defects) dramatically reduced the fraction of the helium which decoupled. Their later experiments[7] showed that the NCRI fraction could be enhanced by growing crystals in narrow channels and by rapid thermal quenching, which is expected to increase defect densities.

Elastic measurements[8–11] also show unusual effects closely related to the TO behavior. The shear modulus decreases by about 10% upon warming to 200 mK, with the same dependence on temperature, amplitude, frequency, and ^{3}He impurity concentration as the NCRI. These modulus effects have a natural interpretation in terms of dislocations, which elastically weaken the crystal at high temperatures where they are mobile but not at low temperatures where they are pinned. Dislocations are created during crystal growth or by plastic deformation and may also provide an explanation of the TO behavior, either through superflow associated with a dislocation network[12–14] or via elastic effects[15] which mimic decoupling. In a recent experiment, a ^{4}He crystal was plastically deformed in the annular gap of a specially designed torsional oscillator.[16] If the increase in TO frequency reflects the decoupling of a supersolid fraction (NCRI) which is associated with crystal defects, then plastic deformation (which increases defect densities) would be expected to raise the TO frequency at low temperatures but not to affect the high-temperature behavior in the normal state. However, the behavior at the lowest temperature was unaffected by deformation. Instead, the high-temperature TO frequency decreased after the deformation. This behavior resembles that of the shear modulus[9] and suggests that the TO frequency changes may have an elastic origin. Although the resonant frequency of a torsional oscillator containing solid helium depends primarily on the oscillator's total moment of inertia, it is also affected by the helium's elastic response. An increase in the elastic stiffness of any part of an oscillator, e.g., in the solid helium's shear modulus, will raise the oscillator's frequency and mimic decoupling. However, simple estimates and detailed numerical modeling[17] of typical TO geometries show that a 30% modulus change in the solid ^{4}He would produce TO frequency changes much smaller than those attributed to decoupling, so changes in the helium's stiffness do not appear to be sufficient to explain the observed NCRI.

Heat capacity measurements[18] in solid ^{4}He show a small, broad peak at temperatures near the onset of the TO and shear modulus anomalies. This may reflect a transition to a new low-temperature state but these data have also been analyzed[19] in terms of a linear T term in the heat capacity, in addition to the usual Debye T^3 contribution. This suggests a glasslike two-level system (TLS) component in the heat capacity. Glassy behavior has also been proposed to explain the mechanical response seen in TO and elastic measurements.[19]

Pressure is another fundamental thermodynamic parameter, with a temperature dependence related to the heat capacity through the Grüneisen equation of state

$$P(T) - P_0 = \sum \frac{\gamma_i}{V} \int C_i dT, \qquad (1)$$

so a Debye T^3 phonon term in the heat capacity produces a T^4 term in the pressure. A linear T term in the heat capacity is expected to produce a T^2 term in the pressure, although the Grüneisen relation for the TLS contributions in glasses[20] is not as well established as it is for phonons in ^{4}He.[21] Pressure measurements[22] in ^{4}He have shown a non-Debye T^2 term which was reduced or eliminated through annealing, as expected if it originated from defects in the solid. Intriguingly, the T^2 pressure term did not appear[23] in measurements on ^{3}He. Other pressure measurements[24] have also shown a T^2 pressure term in crystals grown with the blocked capillary technique, but in this case the non-Debye term decreased only slightly when the crystal was annealed. Also, the measured pressure relaxed slowly, even at the lowest temperatures (19 mK). At higher temperatures the relaxation was faster, consistent with a thermal activation barrier of 28 mK.

During crystal growth at constant volume (the blocked capillary technique used in nearly all TO experiments) the pressure at which the solid is formed drops by about 25 bars. This deforms the crystal and produces defects in the solid helium. In some experiments, subsequent annealing produced large pressure drops which were attributed to changes in density due to elimination of defects[7] or recrystallization of metastable liquid or glassy regions.[22] If the excess volume associated with defects like dislocations could be calculated, this pressure drop would provide a measure of the dislocation density in solid helium, an important parameter for models of supersolidity and one for which we currently have only indirect estimates. However, internal strains in a solid can lead to significant pressure gradients, and pressure changes measured at a single point might be due to a reduction of these gradients rather than to an overall drop in pressure. This would redistribute mass within the cell and could produce changes in the moment of inertia which would affect a torsional oscillator's frequency.

A number of attempts[25–28] to observe mass flow in solid helium in response to a pressure difference showed no evidence of flow at low temperatures, although some flow was seen near melting.[26,27] Recent experiments[29–31] have shown mass flux through solid helium in some samples but in other cases there were stable pressure differences of about 100 mbar across the cell without any apparent flow.

In order to distinguish overall pressure changes associated with elimination of defects from local pressure effects due to changes in pressure gradients, and to better understand annealing processes in solid helium, we have made measurements of the pressure in solid ^{4}He in two locations in a cylindrical cell. By rapidly melting and thermally quenching the helium crystals, we were able to produce pressure differences between the ends of the cell as large as 330 mbars, from which we estimate a yield stress of hcp ^{4}He crystals of roughly 4 kPa. Above about 0.5 K, these pressure gradients decreased at a rate which increased with temperature. The temperature dependence was consistent with a thermally activated process with an activation barrier of about 5 K. Pressure gradients could be almost completely eliminated by annealing near the melting temperature, but we did not observe any significant changes in the average pressure in the cell due to this annealing. In most of our measurements the temperature dependence of the pressure below 700 mK was well described by the Debye T^4 phonon contribution. In a few cases we saw an additional T^2 contribution but this was not reproducible at both ends of the cell, showing that it is difficult to measure the true thermodynamic temperature dependence of the pressure in the presence of pressure gradients.

II. EXPERIMENTAL DETAILS

In these experiments, we created large pressure gradients and defect densities by rapid thermal quenching of solid ^{4}He samples. Our goal was to heat the cell from low temperature to the melting point in a few seconds and to then cool the cell below 0.5 K as quickly as possible. The cylindrical cell is shown schematically in Fig. 1. It is made from oxygen -free high-conductivity copper and has an internal volume of 5.5 cm^3 (length $L = 3.05$ cm, radius $R = 0.76$ cm). Two capacitive pressure gauges ($P1$ and $P2$) are incorporated into the cell's end caps in order to measure pressure differences and were calibrated against each other in the liquid phase at 4.2 K. The end of the cell containing the first pressure gauge ($P1$) was attached to the mixing chamber of our dilution refrigerator via a brass block, whose thermal resistance R determined the cooling rate during thermal quenches. Temperatures were measured with a calibrated germanium sensor, supplemented by a ^{60}Co nuclear orientation thermometer at temperatures below 50 mK. Crystals were grown from ^{4}He (with a nominal ^{3}He concentration of 0.3 ppm) using the blocked capillary technique.

Heat pulses could be applied at the opposite end of the cell (close to gauge $P2$) using an external 1000 Ω heater

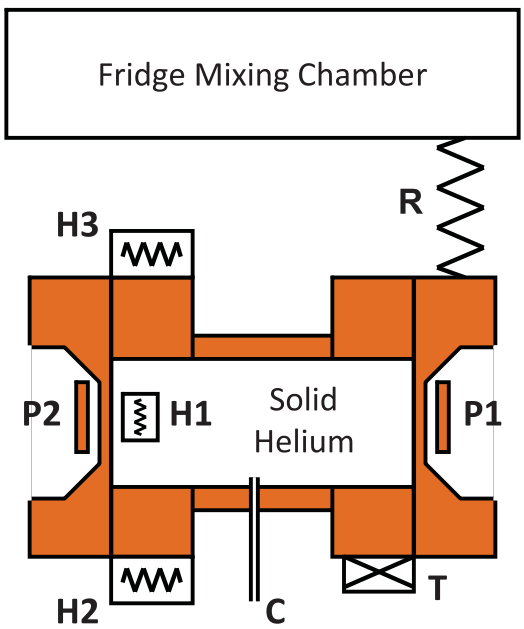

FIG. 1. (Color online) Schematic of the pressure cell attached to the mixing chamber of the dilution refrigerator. $P1$ and $P2$ are capacitive pressure gauges. $H1$ and $H2$ are the internal and external heaters used for applying heat pulses. $H3$ is a 200 Ω heater used for temperature control. T is a calibrated germanium resistance thermometer. The fill capillary C enters at the center of the cell. R is the thermal link between the cell and the mixing chamber.

$H2$ mounted on the cell or using an internal heater $H1$ embedded directly in the solid helium. The internal heater was a 1000 Ω thick film chip resistor, 4×4 mm^2, suspended near the cylinder axis by its electrical leads. Heat pulses were generated by applying dc voltages up to 10 V for times ranging from 1 to 10 s.

When a heat pulse is applied, the response depends on the heat capacities of the solid helium, the copper cell, and the dilution refrigerator's mixing chamber and on the thermal time constants of the different components. The high thermal conductivity of copper results in a very short time constant for relaxation of thermal gradients in the copper cell. It also severely limits the thermal gradients that can be produced in the cell with the external heater. The internal thermal time constant of the solid helium in the cell is somewhat longer, a few tens of milliseconds below 0.5 K. The time constant for thermal equilibrium between the helium and the cell is controlled by the Kapitza resistance between solid helium and copper and is comparable to the helium's internal time constant. Since these time constants are much shorter than our typical heat pulse durations (several seconds), we expect the temperature of the solid helium and cell to be fairly uniform. The internal heater supplies heat directly to the solid helium and so will produce much larger local temperature gradients in the helium. The longest thermal time constant is that between the cell and the mixing chamber of the refrigerator. The mixing chamber's heat capacity is much larger than that of the cell containing helium so this time constant essentially depends on the heat capacity of the cell plus helium and on the conductivity R of the thermal link. The link was chosen to maximize the thermal quench rate after a heat pulse while still allowing us to partially melt the helium before the mixing chamber warms significantly. We estimated time constants of order 1 and 10 s for the two thermal links used in these experiments, although the measured values were somewhat longer because of additional thermal resistances at the clamped surfaces of the link.

III. RESULTS

Starting with high-pressure liquid in the cell, crystals were grown at constant volume using the blocked capillary technique. Figure 2 shows the measured pressure $P2$ during the growth of two such crystals. The higher-pressure crystal began to freeze at a pressure of 57 bars and a temperature of 2.5 K. It then cooled along the ^{4}He melting curve for about 70 min until freezing was complete around 1.77 K and 30.7 bars. After leaving the melting curve in the hcp phase, the pressure along the isochore dropped slightly, to 30.6 bars below 1 K. The second crystal began freezing at 51 bars and 2.35 K, and then was slowly cooled (over about 11 h) until it reached the bcc-hcp triple point at 36 bars and 1.77 K. It then followed the bcc-hcp coexistence curve for 20 min until it entered the hcp phase at about 1.55 K, ending up at a pressure of 27.2 bars.

During blocked capillary growth, the parts of the solid which form first (at high pressure) expand and deform as the pressure decreases along the melting curve. At the end of crystal growth, significant inhomogeneities and pressure gradients may be present in the solid helium, particularly if the freezing is rapid. Figure 3 compares the pressures $P1$ and

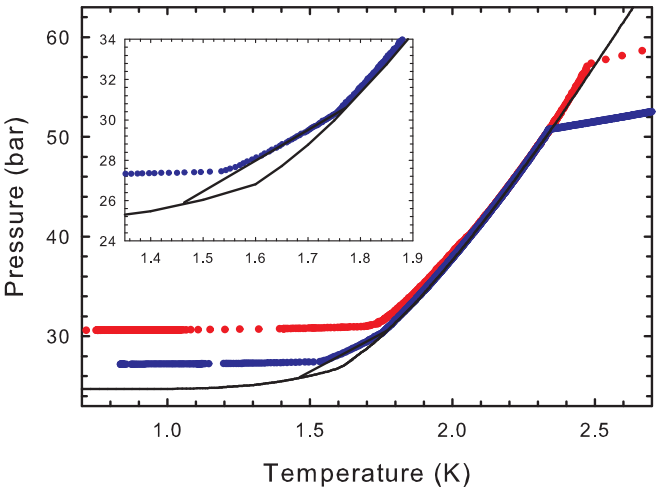

FIG. 2. (Color online) Thermodynamic paths (pressure vs temperature) for constant volume (blocked capillary) growth of two ^{4}He crystals with final pressures of 30.6 and 27.2 bars. The solid lines are the melting curve and bcc-hcp coexistence line for ^{4}He. The inset shows a blowup of the path for the lower-pressure crystal, which undergoes a bcc-hcp transition after freezing.

$P2$ at opposite ends of the cell during melting and freezing of the 30.6 bar hcp crystal. Figure 3(a) shows the pressures when the crystal was warmed at a rate of 0.14 mK/s to 1.95 K (where about 20% of the solid has melted). The onset of melting was sharp and occurred at 1.788 K. Initially there was a pressure difference ΔP of about 10 mbars in the solid, which dropped to less than 1 mbar after melting began. The cell was then cooled [Fig. 3(b)] from 1.95 K at a rate of 0.5 mK/s and the helium was completely refrozen by about 1.76 K. Pressure differences $\Delta P = P2 - P1$ as large as 33 mbars occurred near the end of freezing; these dropped to about 13 mbars upon further cooling.

In order to maximize the pressure gradients and disorder in the crystal, we partially melted and thermally quenched the 30.6 bar crystal as quickly as possible. The density difference between liquid and hcp solid helium at this pressure is about 7%, so melting of even a small fraction of the solid produces pressure differences much larger than we could generate from temperature gradients in solid helium. Figure 4 shows the temperature and the pressures at the two ends of the cell during one such melt-quench cycle. The crystal was initially at a temperature of 50 mK with a small pressure gradient $P1 - P2 = 30$ mbars. A 750 mJ heat pulse (100 mW for 7.5 s) was applied to the internal heater, raising the cell temperature to about 1.86 K. This melted 10% of the crystal and raised the pressures to about 33 bars. Following the heat pulse, the temperature and pressure decreased linearly until freezing was complete, about 30 s after the end of the heat pulse. The solid helium then cooled more rapidly, reaching 0.5 K about 20 s later. This rapid melting and thermal quench increased the pressure difference to $P1 - P2 = 170$ mbars. As expected, melting and quenching raises the pressure $P1$ at the end furthest from the heater since melting near the heater raises the pressure locally. This pushes mass toward the opposite end, leaving a larger pressure $P1$ at that end after quenching.

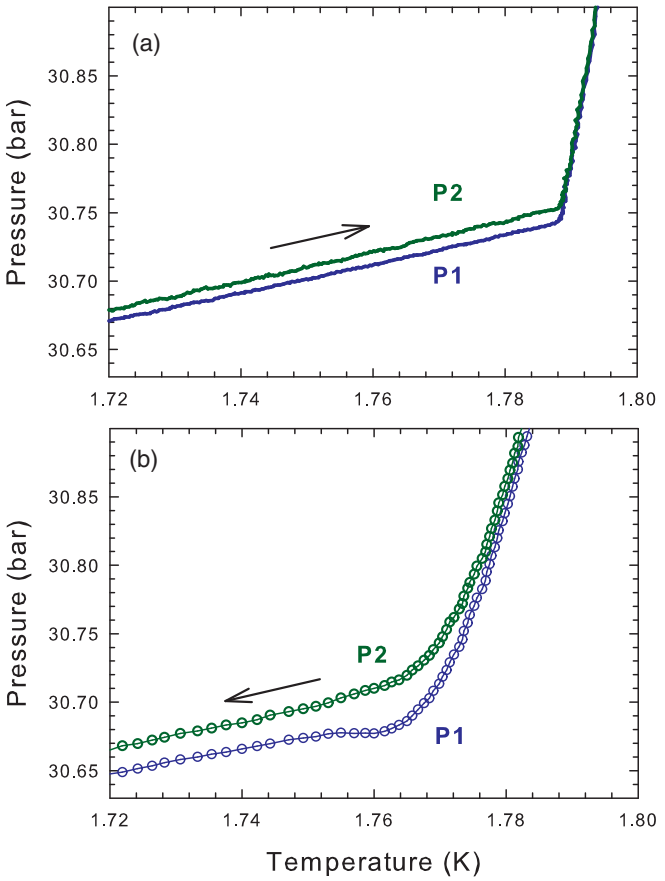

FIG. 3. (Color online) Pressures $P1$ (green symbols) and $P2$ (blue symbols) measured at the two ends of the cell for the 30.6 bar crystal of Fig. 2 during (a) warming and melting and (b) subsequent cooling and freezing.

Substantial pressure changes can also be generated without melting, by heating a lower-pressure crystal into the bcc phase. Figure 5 shows the result for the 27.2 bar crystal of Fig. 2. The crystal was initially at a temperature of 50 mK with a

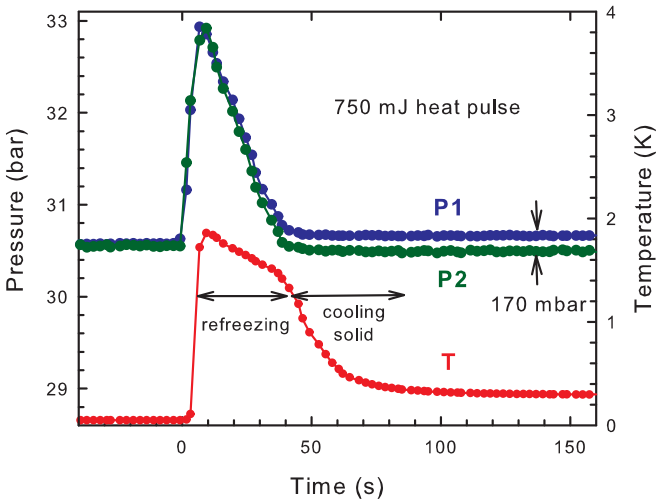

FIG. 4. (Color online) Creation of a pressure gradient by partial melting and thermal quenching of the 30.6 bar ^{4}He crystal. Pressures $P1$ (blue symbols) and $P2$ (green symbols) and temperature (red line) for a 750 mJ heat pulse.

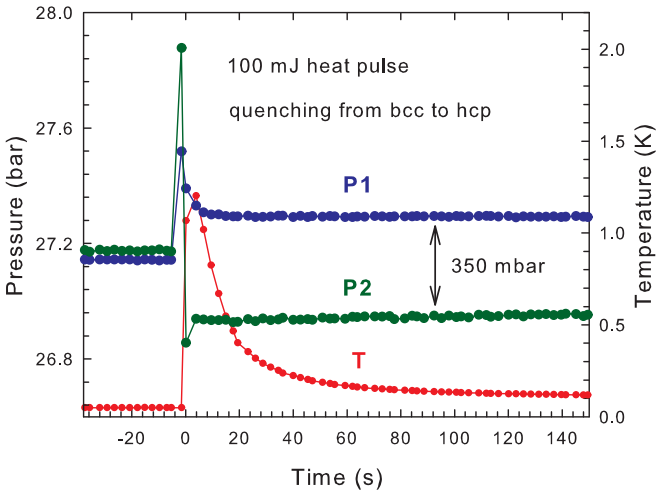

FIG. 5. (Color online) Creation of a pressure gradient by heating the 27.2 bar ^{4}He crystal into the bcc region of the phase diagram. Pressures $P1$ (blue symbols) and $P2$ (green symbols) and temperature (red line) for a 100 mJ heat pulse.

pressure gradient $P2 - P1 = 30$ mbars. A 100 mJ heat pulse (100 mW for 1 s) was applied to the internal heater, raising the cell temperature to about 1.2 K and the pressure $P2$ by about half a bar. The temperature decreased very quickly following the heat pulse, reaching 0.5 K in about 12 s. This process resulted in a pressure difference $P1 - P2 = 350$ mbars, larger than was produced by partial melting of the higher-pressure hcp crystal.

After these thermal treatments, we warmed the quenched helium crystals to study the annealing of the pressure gradients we had created. Figure 6 shows the pressures $P1$ and $P2$ at

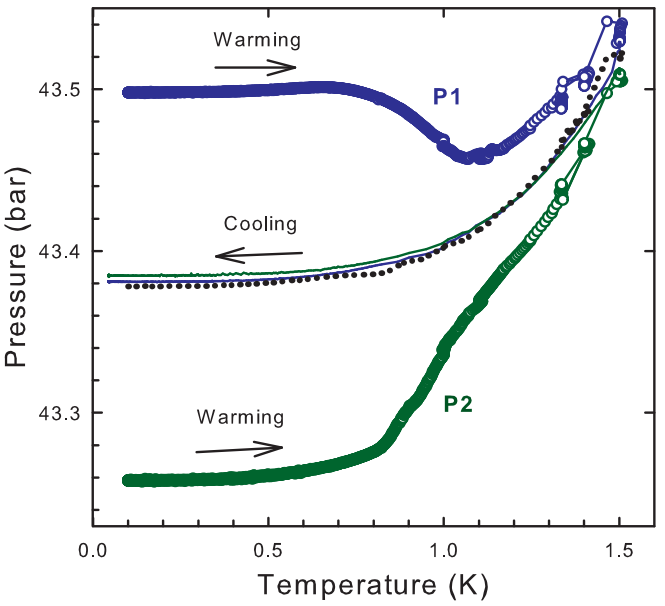

FIG. 6. (Color online) Warming and cooling a 43.4 bar ^{4}He crystal with an initial pressure gradient. Open circles show the pressures $P1$ (blue) and $P2$ (green) during initial warming to 1.5 K. The black dotted line is the average of these two pressures. The solid (blue and green) lines show the pressures $P1$ and $P2$ during subsequent cooling.

the opposite ends of a higher-pressure (43.4 bar) hcp crystal. After applying a 750 mJ heat pulse and thermally quenching the sample, the final pressure difference at low temperatures was $P1 - P2 = 240$ mbars. The crystal was then warmed to 1.5 K over about 25 h. Around 0.5 K the pressures began to change: $P2$ increased while $P1$ (and the pressure difference $P1 - P2$) decreased. By the time the sample reached 1.5 K, annealing had reduced the pressure difference to 20 mbars. The sample was then cooled to 50 mK in 12 h (blue and green solid lines). The pressure difference changed sign below 1.2 K but remained small during cooling, with $P2 - P1 = 4$ mbars at 50 mK. It is clear from Fig. 6 that a drop in pressure measured at a single point during annealing can be misleading. If only the pressure $P1$ had been measured, the pressure drop due to annealing might have been interpreted as being due to the elimination of excess volume associated with defects or liquid droplets in the sample. With two pressure gauges, it is obvious that the main effect of annealing is to eliminate pressure gradients, not to reduce the overall pressure. This is clear from Fig. 6, where we compare $\frac{P1+P2}{2}$ (dotted line), the average of the pressures measured during warming, to the pressures $P1$ and $P2$ measured while cooling after the anneal. Annealing does not change the average pressure significantly—it actually increases slightly. Of course, even measuring the pressures at two points does not give the overall average pressure in the cell.

We studied the annealing of pressure gradients in more detail by changing the sample temperature in discrete steps. Figure 7 shows the pressures $P1$ and $P2$ for the 30.6 bar crystal of Figs. 3 and 4. After partial melting and thermal quenching to create a large pressure gradient (264 mbars), the crystal was warmed from 55 to 100 mK, and then in 100 mK steps to 900 mK, holding the temperature constant for about 35 min at each step. Above 0.5 K, the pressures began to change at a rate which increased rapidly with temperature. By the time the

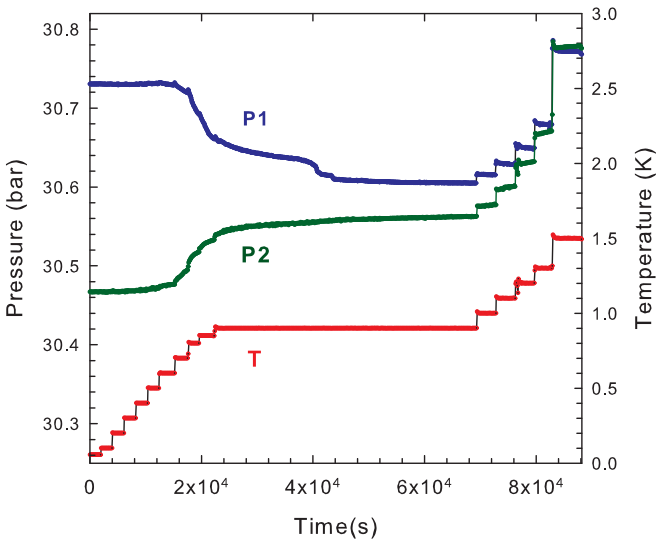

FIG. 7. (Color online) Annealing of a pressure gradient in the 30.6 bar ^{4}He crystal (melting temperature 1.79 K) during stepwise warming. The upper (blue and green) data (left axis) are the pressures $P1$ and $P2$ as functions of time; the lower (red) curve (right axis) is the corresponding temperature.

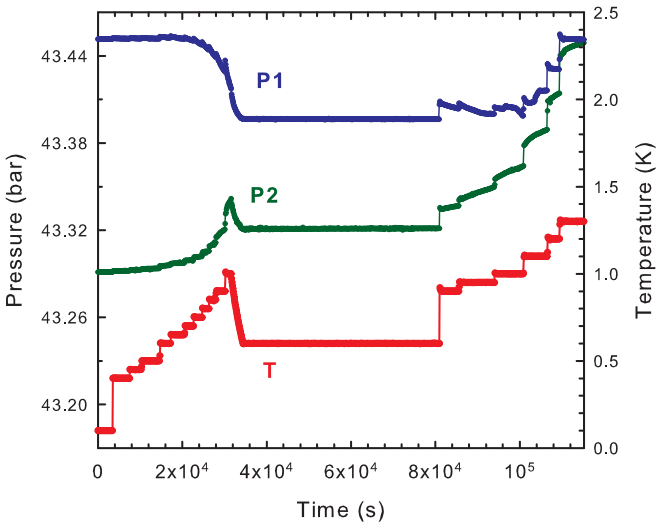

FIG. 8. (Color online) Annealing of a pressure gradient in a 43.4 bar ^{4}He crystal (melting temperature 2.15 K) during stepwise warming. The upper (blue and green) data (left axis) are the pressures $P1$ and $P2$ as functions of time; the lower (red) curve (right axis) is the corresponding temperature.

temperature reached 900 mK, the pressure difference $P1 - P2$ had been reduced by more than 50%, to 120 mbars. We then held the temperature constant at 900 mK for 13 h, during which time the pressure difference decreased to 43 mbars but then stabilized. To further reduce the pressure difference, we then raised the temperature in steps to 1.5 K, where the two pressures became equal. When we waited at 1.5 K, the pressure difference reversed, leaving a small 8 mbar pressure difference in the opposite direction. The fact that a pressure difference reappears after the pressures $P1$ and $P2$ were equal indicates that the pressure distribution within the solid was inhomogeneous.

Figure 8 shows the analogous behavior for the 43.4 bar crystal of Fig. 6. Starting from an initial pressure difference of 160 mbars, the temperature was raised in steps. Again, the pressure difference began to decrease above 500 mK. At

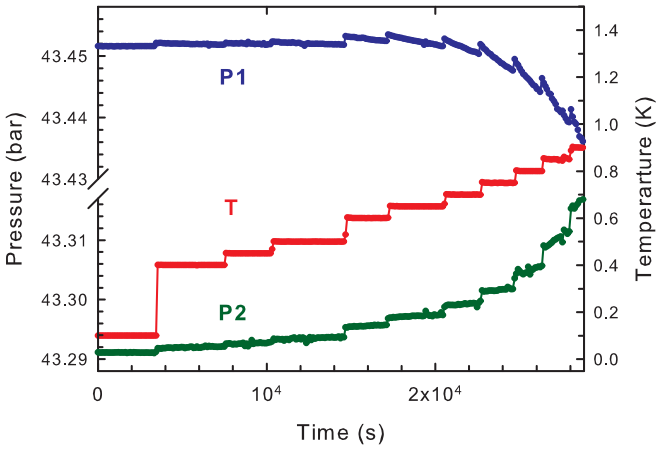

FIG. 9. (Color online) Blowup of the initial portion of Fig. 8, for temperatures up to 0.7 K. Note the break in the pressure (left) axis.

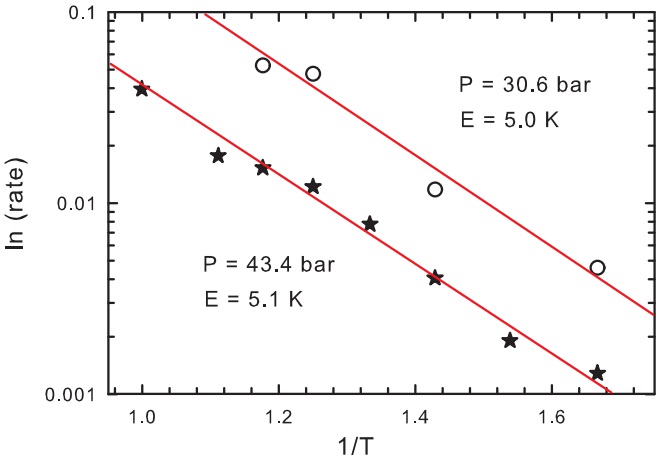

FIG. 10. (Color online) Arrhenius plot [ln(rate) vs $1/T$] of the annealing rates for the 30.6 bar (open circles) and 43.4 bar (solid stars) crystals of Figs. 7 and 8. Solid lines are linear fits corresponding to activation energies of 5.0 and 5.1 K, respectively.

the maximum temperature of 1.3 K, the pressure difference was only 1 mbar. The rate at which the pressure difference changed during annealing increased rapidly with temperature. The slope of $P1$ vs temperature is a measure of the rate of annealing and Fig. 9 shows these pressure changes on an expanded scale.

In Fig. 10 we plot the logarithm of the slope $\frac{dP1}{dt}$ vs $\frac{1}{T}$ for the crystals of Figs. 7 and 8. Using the pressure difference $P1 - P2$ gives essentially the same result but with more scatter since the $P2$ data are noisier. The data for each crystal fall on a straight line in this Arrhenius plot, showing that the annealing of pressure gradients in the temperature range 0.5 to 1 K is a thermally activated process. The slopes give similar activation barriers for the two crystals: 5.0 K for the 30.6 bar crystal and 5.1 K for the 43.4 bar crystal.

In addition to studying the effects of thermal quenching and annealing on pressure gradients, we also attempted to look for a T^2 defect contribution to the temperature dependence of the pressure. Figure 11(a) shows the pressures $P1$ and $P2$ at low temperatures for the 43.4 bar crystal of Figs. 6 and 8 during its initial cooling (following blocked capillary growth). The two pressures differ by $P2 - P1 = 43$ mbars but their temperature dependences are similar. Both $P1$ and $P2$ are well described by $P(T) = P_0 + aT^2 + bT^4$, as shown by plotting the same data as $\frac{P-P_0}{T^2}$ vs T^2 in Fig. 11(b). The slopes of the straight lines (the coefficients b corresponding to the Debye T^4 pressure term) are essentially the same for the pressures measured at the two ends of the cell. However, the intercepts (the magnitude of the non-Debye T^2 term) seem to be different at the two ends. The $P2$ data have a nonzero intercept of about 0.0017 bars/K^2, similar to the value seen in other measurements.[22,24] However, the $P1$ data from the opposite end of the cell (which is less noisy) have essentially zero intercept, i.e., $P1$ is described by the Debye T^4 dependence alone. This was true for almost all our pressure measurements in different crystals—only one of our five other crystals showed a nonzero T^2 term in pressure (a T^2 term of 0.0018 bars/K^2 in a 30.5 bar crystal after partial melting and thermal quenching).

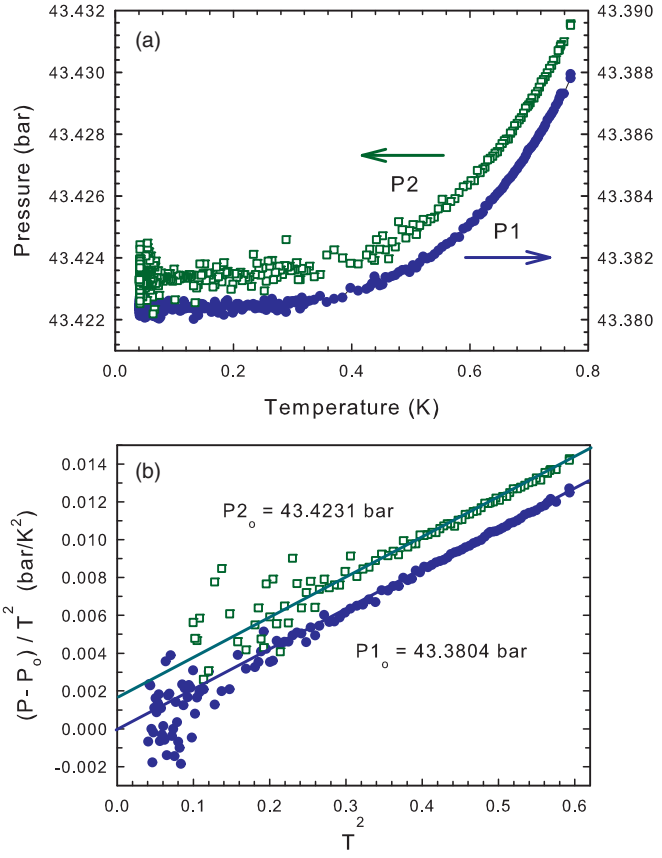

FIG. 11. (Color online) Temperature dependence of the pressure in the 43.4 bar crystal. (a) Pressures $P1$ (open green squares) and $P2$ (solid blue circles) vs temperature. Note the different pressure axes for $P1$ and $P2$. (b) $(P - P_0)/T^2$ vs T^2 for $P1$ and $P2$, showing the $aT^2 + bT^4$ dependence of the pressure.

We also observed unexpected pressure dependences in some samples. For example, in one crystal the coefficient of the Debye T^4 term changed by a factor of 2 when the crystal was warmed and then cooled. In another case, during cooling the pressure $P2$ increased below 250 mK (by about 3 mbars) while $P1$ remained constant at the other end.

IV. DISCUSSION

Pressure gradients in a solid require nonzero shear stresses. These are limited by the crystal's yield stress—the maximum shear stress that can be sustained without plastic flow. However, the mechanisms by which a crystal can plastically deform depend on the strain rate $\frac{d\epsilon}{dt}$, as well as on the temperature and previous history of the solid, so there is no single well-defined yield stress for a material. In measurements like ours, pressure gradients are created or measured over time scales from seconds to hours, and it is the flow stress at strain rates $\frac{d\epsilon}{dt} \sim 10^{-2}$–$10^{-7}$ s^{-1} that is relevant.

Many different mechanisms can contribute to plastic deformation. Close to melting, thermally activated vacancy creep may be important at low strain rates but at lower temperatures the motion of dislocations[32] dominates. For small stresses and strains, deformation occurs via the bowing out of dislocations between pinning points. As the stress increases, dislocations break away from impurity pinning sites, increasing the

deformation but not creating new dislocations or irreversibly changing the dislocation network. At even higher stresses, dislocations bow out further and, depending on the dislocation density, may intersect other dislocations. If they pass through each other—a process known as forest cutting—jogs are produced on each dislocation and can provide additional pinning points. However, for large plastic deformations the most important effect is dislocation multiplication, in which Frank-Read sources create new dislocation loops which remain after the stress is removed. Irreversible phenomena like yield drop (reduction of plastic flow stress because of dislocation multiplication) and work hardening (increased flow stress due to intersections and pinning in high-density dislocation networks) are often observed.

The new defects created by plastic deformation can only be removed by annealing at high temperatures. For example, the elimination of dislocations via climb (the motion of an edge dislocation perpendicular to its Burgers vector) requires mass transport from the bulk lattice to the dislocation. This normally occurs via vacancy motion and therefore requires temperatures high enough to create significant numbers of thermal vacancies. It has been suggested that superflow along dislocation cores could provide an additional, nonthermal climb mechanism in solid helium, a phenomenon dubbed superclimb.[33] Climb is an important process for annealing away edge dislocations and it also allows jogs to move along a dislocation and disappear, eliminating them as pinning sites. However, it does not have the same effects on screw dislocations, which are often much harder to anneal away. Plastic deformation often produces a dense tangle of edge and screw dislocations, with many intersections and pinning sites, and it is generally not possible to return the crystal to its original, low-defect-density state by annealing, even by holding it close to its melting temperature for an extended period.

Large-scale plastic flow involves dislocations moving in response to shear stresses in their slip planes. Although dislocations may glide easily in some crystallographic directions, a general plastic deformation involves motion along several different slip systems. In hexagonal crystals like helium, a minimum of five different slip systems are needed to ensure continuity of the solid when, for example, an object is pulled through a crystal or a polycrystal is deformed. In such cases, the flow will be controlled by the slip system with the largest yield stress. Early experiments[34,35] in which a steel ball was pulled through solid ^{4}He at 32 bars and 1.5 K gave flow stresses of order 2 to 6 kPa at strain rates of $\frac{d\epsilon}{dt} \sim 10^{-5}$ –10^{-3} s^{-1}. If there is liquid present at crystal surfaces or grain boundaries, continuity constraints are relaxed and deformation can occur on the easiest slip systems, at lower stresses. This effect was seen in plastic deformation experiments on constrained hcp and bcc ^{4}He single crystals near their melting temperatures.[36,37] These gave yield stresses of 20 to 120 kPa at strain rates of $\frac{d\epsilon}{dt} \sim 10^{-3}$–$10^{-4}$ s^{-1}. However, when a thin layer was melted at the crystals' sides, deformation occurred at stresses below the experimental resolution of 3 kPa. This implies that the pressure differences and stresses which can be sustained during crystal growth (when there is liquid present) are smaller than those which can occur in the solid off the melting curve.

In our experiments, the largest pressure differences we observed with any liquid in the cell were about 40 mbars and these were typically much smaller (∼1 mbar) when a crystal was melted slowly. At the completion of blocked capillary crystal growth, we saw pressure differences of order 30 mbars and these persisted to low temperatures unless cooling was very slow. By rapidly melting some of the solid, followed by freezing and thermal quenching, we were able to generate pressure differences up to 240 mbars (Fig. 6). Even larger pressure differences (330 mbars) were generated by rapidly heating a lower-pressure crystal into the bcc phase without any melting (Fig. 5), supporting the idea that the presence of liquid in the cell limits the maximum pressure gradient that can be sustained.

An estimate of the yield stress σ_c of solid helium can be obtained from the observed pressure differences in the cell. If a large pressure difference is applied between the opposite ends of a long cylindrical cell (length L and radius R), the helium will flow plastically until the force from the pressure difference ΔP between the ends of the helium cylinder, $\pi R^2 \Delta P$, is balanced by the maximum force from the shear stress at the side walls, $2\pi RL\sigma_c$. This gives a maximum pressure difference (the extrusion pressure) $\Delta P_{\max} = 2\frac{L}{R}\sigma_c$. In our cell, with $\frac{L}{R} = 4.0$, the largest pressure difference we were able to generate (by heating into the bcc phase and quenching) was $\Delta P_{\max} = 330$ mbars, which corresponds to a yield stress $\sigma_c \approx 4.1$ kPa (41 mbars). The pressure differences generated by blocked crystal growth or by partial melting and quenching of hcp crystals were smaller, which could be due to rapid annealing at high temperatures during the thermal quench or could reflect a smaller yield stress at the melting curve.

Note that the maximum pressure difference depends on cell geometry. For example, for a typical fill capillary (with an L/R ratio of 1000), a yield stress of 4.1 kPa lets the capillary sustain a pressure difference of about 80 bars (which allows crystals to be grown using the blocked capillary technique without the solid helium plug slipping). In recent flow experiments[30] in a cylindrical cell of radius 0.32 cm, a pressure difference was applied to solid ^{4}He through superfluid in Vycor rods $L = 2.06$ cm apart. In some cases there was no flow and static pressure differences up to about 450 mbars were observed, close to the maximum predicted pressure difference $\Delta P_{\max} = 2\frac{L}{R}\sigma_c = 530$ mbars.

A similar calculation can be done for other geometries. For a thin annulus (gap $t \ll$ length L), the maximum pressure difference is $\Delta P_{\max} = 2\frac{L}{t}\sigma_c$. The helium sample which showed the largest apparent NCRI in TO experiments[7] was grown using the blocked capillary method in an annular oscillator with a narrow gap $t = 0.15$ mm. When the crystal was annealed, the pressure dropped by 7 bars, which the authors suggested could reflect the elimination of defects and the inflationary pressure associated with them. However, for the ratio $L/t = 73$ of this annulus, a yield stress of 4.1 kPa gives a maximum pressure difference about 6 bars, suggesting that most of the observed pressure change may be due to annealing of pressure gradients, not elimination of excess volume associated with defects.

An analogous calculation can also be done for a disk geometry, (a cylindrical cell with height $H \ll$ radius R)

for which the maximum pressure difference between the center and the outer edge is $\Delta P_{\max} = 2\frac{R}{H}\sigma_c$. In a cell used for pressure relaxation studies,[24] the ratio $R/H = 172$ gives a maximum pressure difference of 7 bars, roughly the same as the 6 bar pressure drop observed when a crystal was annealed in this cell. In a cell used for plastic deformation pressure studies,[38] $R/H = 35$, giving a maximum pressure difference of about 3 bars. By applying an excess pressure greater than 5 bars at the center of the cell, the authors were able to deform the sample and produce an increase in the glassy T^2 term in the temperature dependence of the pressure. However, applied pressures of less than 3 bars did not show such an effect, which might be anticipated since these pressures would not generate stresses large enough to produce plastic flow.

All the experiments discussed above appear to be consistent with a yield stress of order 4000 Pa (40 mbars). This is much larger than the stress at which the shear modulus shows amplitude dependence[10] associated with the breakaway of dislocations from ^{3}He impurity pinning sites ($\sim$8 Pa). It is also larger than the 700 Pa acoustic stresses which changed the shear modulus[9] of solid ^{4}He. However, those changes were completely reversed by warming the crystal to 600 mK while the pressure gradients we created by thermal quenching annealed much more slowly and could only be eliminated at temperatures above 1 K.

The pressure gradient annealing began at 500 mK and the annealing rate increased rapidly with temperature. As shown in Fig. 10, the annealing rate was thermally activated with an energy barrier of about 5 K. This is much larger than the 28 mK activation energy found[24] for pressure relaxation at temperatures below 300 mK. However, the total pressure change associated with that relaxation was only about 0.1 mbars and so would not have been resolvable in our experiments. The 5 K energy barrier is also much larger than the 0.7 K energy for unpinning of dislocations from ^{3}He impurities,[11] which was measured at much lower stresses ($<$0.2 Pa). It appears to be associated with the annealing of defects created by plastic deformation during crystal growth or subsequent thermal quenching. As discussed above, these could be jogs created on existing dislocations when they intersect with other dislocations or they could be new edge and screw dislocations created by the deformation. In the case of jogs, thermal vacancies can allow them to move along dislocations and, for example, annihilate with antijogs. Since jog motion is nonconservative, i.e., involves mass transport, the relevant activation energy is that of mobile vacancies. Nuclear magnetic resonance and other measurements[39] give experimental values of the activation energy for vacancy motion in helium which range from about 8 to 16 K at pressures near melting. Recent computations[40] give a value of 13 K at the melting density. The observed 5 K activation energy is somewhat smaller than these values, but activation energies for motion of vacancies along dislocation cores (pipe diffusion) are often significantly smaller than the bulk values. The climb of dislocations due to jogs moving along them is an important mechanism in annealing, particularly of edge dislocations. The fact that the activated pressure relaxation we observe between 500 mK and 1 K does not completely eliminate pressure gradients may reflect the greater stability of screw dislocations or high-density dislocation tangles and grain boundaries. At higher temperatures, other processes assist in annealing so that the pressure gradients become much smaller, but there is no reason to believe that all the dislocations and other defects have been eliminated.

The non-Debye behavior and other unexpected effects we observed in the temperature dependence of the pressure, $P(T)$, may simply reflect annealing of pressure gradients. From Figs. 7 to 9 it is obvious that significant time-dependent pressure changes occur above 500 mK. These would affect the apparent Debye T^4 term which is extracted from $P(T)$ in the range 0.4 to 0.7 K. It is clear that it is difficult to extract reliable information about the thermodynamic temperature dependence of the pressure, $P(T)$, in the presence of pressure gradients and annealing. Our cell is quite an open one—pressure gradients would be even bigger in annular or pancake-shaped cells with larger aspect ratios.

Annealing crystals removes most of the pressure gradients but would also eliminate many of the defects presumed to be responsible for the T^2 term in $P(T)$. It is possible that the thermodynamic temperature dependence of P could be determined in the presence of pressure gradients by restricting the measurements to temperatures well below 500 mK, where the thermally activated annealing we observed is negligible. However, this puts more stringent requirements on the resolution of the pressure measurements and, given the relaxation observed by Rittner and Reppy below 300 mK, this may still not be possible. Measurements made with a single pressure gauge should be interpreted with caution, especially if the samples were grown or deformed in such a way as to produce large pressure gradients.

ACKNOWLEDGMENT

This work was supported by NSERC Canada.

[1] A. F. Andreev and I. M. Lifshitz, Sov. Phys. JETP **29**, 1107 (1969).
[2] G. V. Chester, Phys. Rev. A **2**, 256 (1970).
[3] A. J. Leggett, Phys. Rev. Lett. **22**, 1543 (1970).
[4] E. Kim and M. H. W. Chan, Nature (London) **427**, 225 (2004).
[5] E. Kim and M. H. W. Chan, Science **305**, 1941 (2004).
[6] A. S. C. Rittner and J. D. Reppy, Phys. Rev. Lett. **97**, 165301 (2006).
[7] A. S. C. Rittner and J. D. Reppy, Phys. Rev. Lett. **98**, 175302 (2007).
[8] J. Day and J. Beamish, Nature (London) **450**, 853 (2007).
[9] J. Day, O. Syshchenko, and J. Beamish, Phys. Rev. B **79**, 214524 (2009).
[10] J. Day, O. Syshchenko, and J. Beamish, Phys. Rev. Lett. **104**, 075302 (2010).
[11] O. Syshchenko, J. Day, and J. Beamish, Phys. Rev. Lett. **104**, 195301 (2010).

[12]M. Boninsegni, Kuklov, L. A. B. Pollet, N. V. Prokof'ev, B. V. Svistunov, and M. Troyer, Phys. Rev. Lett. **99**, 035301 (2007).
[13]S. I. Shevchenko and D. V. Fil, Phys. Rev. B **100**, 100501 (2009).
[14]J. Toner, Phys. Rev. Lett. **100**, 035302 (2008).
[15]I. Iwasa, Phys. Rev. B **81**, 104527 (2010).
[16]J. D. Reppy, Phys. Rev. Lett. **104**, 255301 (2010).
[17]A. C. Clark, J. D. Maynard, and M. H. W. Chan, Phys. Rev. B **77**, 184513 (2008).
[18]X. Lin, A. C. Clark, Z. G. Cheng, and M. H. W. Chan, Phys. Rev. Lett. **102**, 125302 (2009).
[19]J. J. Su, M. Graf, and A. Balatsky, Phys. Rev. Lett. **105**, 045302 (2010).
[20]D. A. Ackerman, A. C. Anderson, E. J. Cotts, J. N. Dobbs, W. M. MacDonald, and F. J. Walker, Phys. Rev. B **29**, 966 (1984).
[21]D. O. Edwards and R. C. Pandorf, Phys. Rev. **140**, A816 (1965).
[22]V. N. Grigor'ev, V. A. Maidanov, V. Y. Rubanskii, S. P. Rubets, E. Y. Rudavskii, A. Rybalko, Y. V. Syrnikov, and V. A. Tikhii, Phys. Rev. B **76**, 224524 (2007).
[23]A. A. Lisunov, V. A. Maidanov, V. Y. R. Rubanskyi, S. P. Rubets, E. Y. Rudavskii, A. S. Rybalko, and V. A. Tikhiy, Phys. Rev. B **83**, 132201 (2011).
[24]A. S. C. Rittner and J. D. Reppy, J. Phys.: Conf. Ser. **150**, 032089 (2009).
[25]D. S. Greywall, Phys. Rev. B **16**, 1291 (1977).
[26]J. Day, T. Herman, and J. Beamish, Phys. Rev. Lett. **95**, 035301 (2005).
[27]J. Day and J. Beamish, Phys. Rev. Lett. **96**, 105304 (2006).
[28]A. S. C. Rittner and J. D. Reppy, Phys. Rev. B **80**, 224516 (2009).
[29]M. W. Ray and R. W. Hallock, Phys. Rev. Lett. **100**, 235301 (2008).
[30]M. W. Ray and R. W. Hallock, Phys. Rev. B **79**, 224302 (2009).
[31]M. W. Ray and R. W. Hallock, Phys. Rev. Lett. **105**, 145301 (2010).
[32]J. P. Hirth and J. Lothe, *Theory of Dislocations*, 2nd ed. (John Wiley and Sons, New York, 1982).
[33]S. G. Soyler, A. B. Kuklov, L. Pollet, N. V. Prokof'ev, and B. V. Svistunov, Phys. Rev. Lett. **103**, 175301 (2009).
[34]H. Suzuki, J. Phys. Soc. Jpn. **35**, 1472 (1973).
[35]H. Suzuki, J. Phys. Soc. Jpn. **42**, 1865 (1977).
[36]D. J. Sanders, H. Kwun, A. Hikata, and C. Elbaum, Phys. Rev. Lett. **39**, 815 (1977).
[37]D. J. Sanders, H. Kwun, A. Hikata, and C. Elbaum, Phys. Rev. Lett. **40**, 458 (1978).
[38]I. A. Degtyarev, A. A. Lisunov, V. A. Maidanov, V. Y. Rubanskiy, S. P. Rubets, E. a. RUdavskii, a. S. Rybalko, and V. A. Tidhii, J. Exp. Theor. Phys. **111**, 619 (2010).
[39]B. A. Fraas, P. R. Granfors, and R. O. Simmons, Phys. Rev. B **39**, 124 (1989).
[40]M. Boninsegni, Kuklov, L. A. B. Pollet, N. V. Prokof'ev, B. V. Svistunov, and M. Troyer, Phys. Rev. Lett. **97**, 080401 (2006).